N95-27990

MEASUREMENT AND PREDICTION OF BROADBAND NOISE FROM LARGE HORIZONTAL AXIS WIND TURBINE GENERATORS

By

F. W. Grosveld & K. P. Shepherd, The Bionetics Corporation
and
H. H. Hubbard, VARC

ABSTRACT

A method is presented for predicting the broadband noise spectra of large wind turbine generators. It includes contributions from such noise sources as the inflow turbulence to the rotor, the interactions between the turbulent boundary layers on the blade surfaces with their trailing edges and the wake due to a blunt trailing edge. The method is partly empirical and is based on acoustic measurements of large wind turbines and airfoil models. Spectra are predicted for several large machines including the proposed MOD-5B. Measured data are presented for the MOD-2, the WTS-4, the MOD-OA, and the U.S. Windpower Inc. machines. Good agreement is shown between the predicted and measured far field noise spectra.

INTRODUCTION

Acoustic measurements are presented for four different horizontal axis machines and are compared with the results of an improved method of predicting broadband noise. This information is considered pertinent for the evaluation of environmental impact on communities located near wind turbine generators operated for large scale electric power generation.

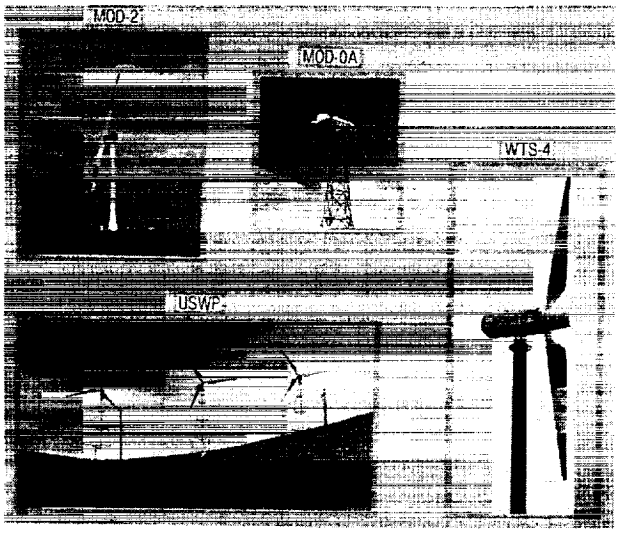

Figure 1. - Photographs of wind turbine generators for which acoustic measurements are presented.

The machines for which data are presented here and in References 1 through 6 are shown in the photographs of Figure 1. They consist of the MOD-2, the MOD-OA, the WTS-4 and the U.S. Windpower machine. The first three of these are government sponsored. All are self starting, have 2 or 3 blades, rotate in the range 17 to 72 rpm, and normally operate at wind speeds of 3 to 16 m/s.

Some dimensions and operational details are included in the table of Figure 2. MOD-2 is noted to be an upwind machine whereas the others are downwind machines. Rotor diameters range from 17.1 m to 91.4 m, rotor tip speeds from 66.5 to 122.4 m/s, blade areas from 15 to 236 m^2, and rated power outputs from 50 to 4200 kW. Calculated values are included for the proposed MOD-5B machine for which data are listed at the bottom of Figure 2.

DESIGNATION	TYPE	ROTOR DIAM, m	TIP SPEED, m/s	BLADE AREA, m^2	RATED POWER, kW
MOD-2	UPWIND	91.4	83.8	236	2500
WTS-4	DOWNWIND	78.4	122.4	195	4200
MOD-0A	DOWNWIND	38.1	80	28	200
USWP	DOWNWIND	17.1	66.5	15	50
MOD-5B	UPWIND	97.6	89.4	230	3200

Figure 2. - Dimensions and operating conditions for several large machines.

NOISE MEASUREMENTS AND OBSERVATIONS

The machines described in Figures 1 and 2 represent wide ranges of size, output power rating and configuration. Resulting differences in their noise production are presented in Figures 3 through 8. Comparisons are made on the basis of one-third octave band spectra, narrow band spectra, dB(A) levels, and perception distances.

Effects of Size and Configuration

The one-third octave band spectra of Figure 3 were measured on axis and normalized to a distance of 100 m from each machine. Definite trends are observed. The spectra exhibit their highest levels at the low frequencies, with general reductions in level as frequency increases. Further, the machines having the highest power output also have the

highest noise levels. This latter trend is particularly evident at the low frequencies.

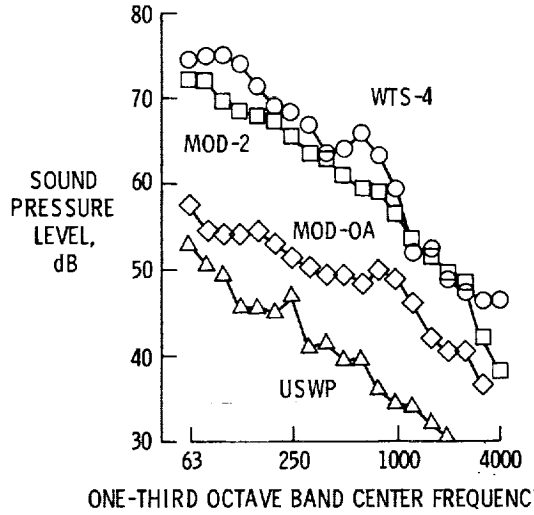

Figure 3. - Measured on-axis noise spectra at approximately rated power for four machines. (r = 100 m.)

A comparison of the narrow band noise spectra for large upwind and downwind machines is given in Figure 4. Data are narrow band (Δf = 0.25 Hz) and are limited to the frequency range below 100 Hz. The general reduction in level with frequency is seen to be about the same for both machines. The WTS-4 machine has a number of discrete peaks in its spectrum, particularly below 50 Hz. These are loading harmonics which occur at integral multiples of the blade passage frequency. Their amplitudes are enhanced because of the tower wake-blade interference encountered in this downwind configuration. In the MOD-2 spectrum only a few discrete peaks are evident and these are believed to be of electromechanical origin. No loading noise harmonics are apparent for this upwind configuration. The relatively lower levels of the MOD-2 spectrum are due in part to its lower tip speed.

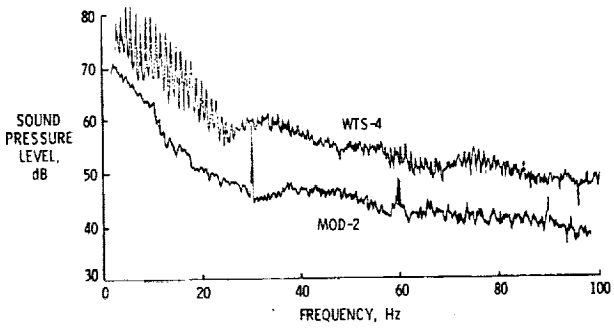

Figure 4. - Comparison of narrow band (Δf = 0.25 Hz) noise spectra at rated power, on axis, for the MOD-2 and WTS-4 machines. (r = 150 m.)

Effects of Output Power

The one-third octave band spectra of Figure 5 illustrate the differences in the noise output for the WTS-4 machine at two different power outputs. Data are for the on-axis measuring points for power outputs of 1,000 and 4,000 kW respectively. Higher levels are associated with the higher power output and are seen to occur at frequencies below about 1,000 Hz.

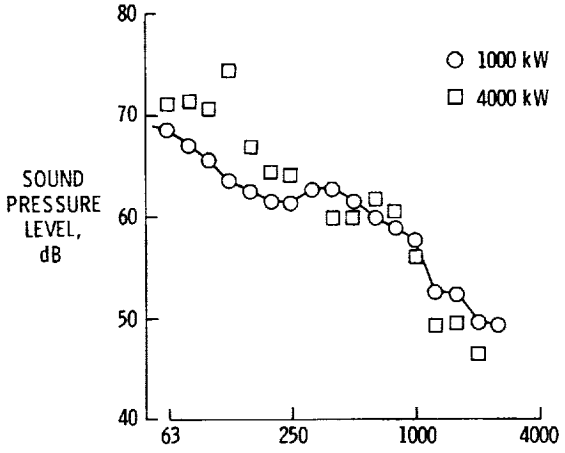

Figure 5. - Effects of power output on noise spectra measured on axis for the WTS-4 machine. (r = 150 m.)

Directivity Effects

Noise measurements for the machines of Figure 1 indicate that the noise radiation patterns are not sharply directional. At equal distances on-axis (upwind and downwind) essentially no differences are observed in either spectral shapes or sound levels. There are, however, consistent differences between measurements made on-axis and in the plane of rotation. Figure 6 shows one-third octave band spectra for the MOD-2 machine. Note that the in-plane data have relatively lower levels at low frequencies and higher levels at high frequencies than do the on-axis data. The result is a cross-over effect as seen in the figure.

Similar data are presented in Figure 7 to show a comparison between the MOD-2 and WTS-4 machines. The data points represent mean L_{eq} (dB(A)) levels for a large number of measurements for both machines. The noise radiation pattern curves in each case are estimated. The MOD-2 machine radiates essentially in a non-directional pattern. The WTS-4 radiation pattern on the other hand shows higher levels on-axis than in-plane. As suggested in Figure 6 the low frequency components are known to be relatively strong on-axis. Thus the skewness of the radiation pattern of the WTS-4 is due to the influence

of the low frequencies on the L_{eq} values.

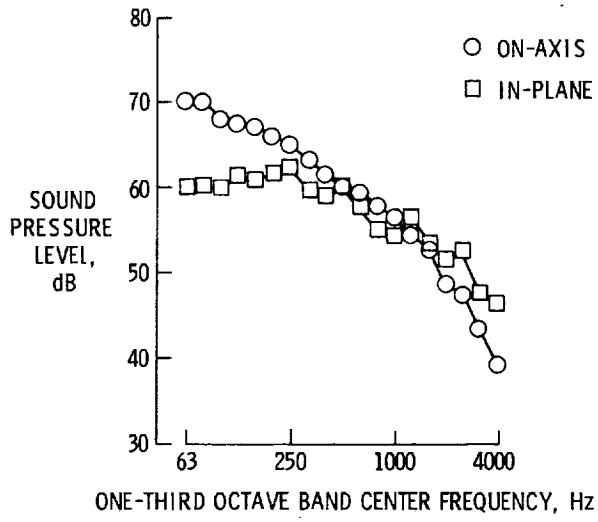

Figure 6. - Comparison of on axis and in plane noise spectra for MOD-2 machine. (P = 2500 kW, r = 100 m.)

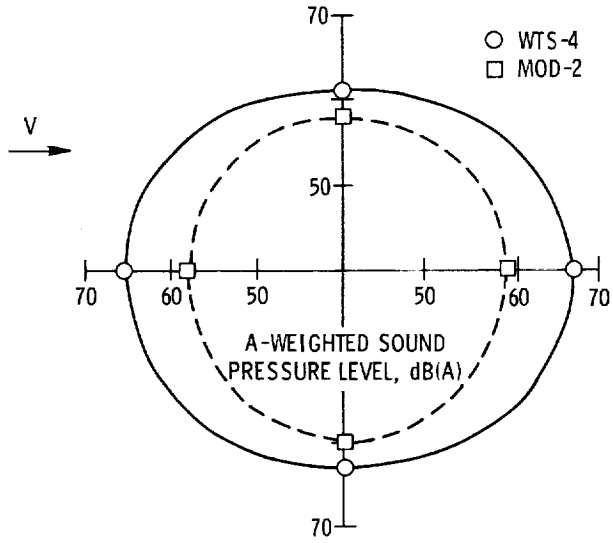

Figure 7. - Comparison of a-weighted noise radiation patterns for WTS-4 and MOD-2 machines. (V_w = 7.6-13.4 m/s, r = 150 m.)

Perception Distances

Observations of the radiated noise from a number of different machines and for a range of weather conditions have established a wind related directionality which is illustrated in Figure 8. The data points for the MOD-2 and the WTS-4 machines represent locations at which the noise during steady state operations is observable intermittently.

Note that the noise is observed at a much greater distance downwind than upwind, in spite of the fact that the noise radiation patterns of Figure 6 are nearly symmetrical. This skewness is due to refraction effects of the mean wind speed gradient, resulting in the formation of shadow zones upwind and propagation enhancement downwind. The distance from the machine to the shadow zone is dependent upon the height of the noise source above the ground surface and the wind speed gradient.

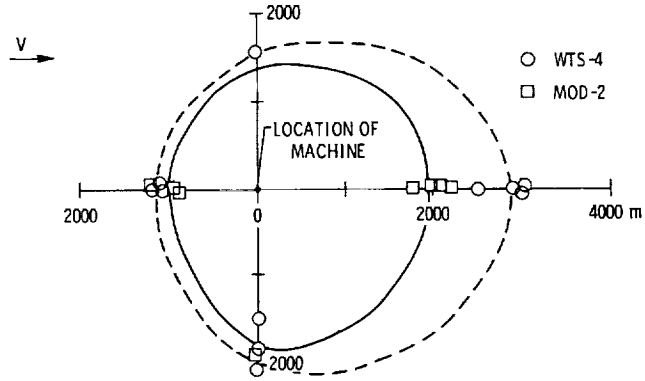

Figure 8. - Comparisons of perception distances for the WTS-4 and MOD-2 machines. (V_w = 7.6-13.4 m/s.)

BROADBAND NOISE PREDICTION

To adequately assess the impact of the wind turbine noise and to aid in the design and siting of machines that are acceptable to the community (Refs. 7 and 8), a thorough understanding of the underlying noise generation phenomena as well as prediction techniques are highly desirable. Current literature on wind turbine noise is limited. Most publications deal with the impulsive "thumping" noise caused by the blade cutting the wake behind its supporting tower, where the rotor is located downwind from the tower (Refs. 9-15). A prediction code for this type of noise is presented in Reference 16. Other possible sources of wind turbine noise are discussed in Reference 5 and some of these noise mechanisms are considered in References 1, 6, and 17-19. Reference 19 compares theory with experimental broadband noise data (Refs. 1 and 2) but results indicate that better prediction techniques are needed. In the next sections a broadband noise prediction scheme for horizontal axis wind turbine generators is presented.

Extensive noise measurements on current, large, horizontal axis wind turbine generators (Refs. 1-6) indicate the presence of three major aerodynamic source mechanisms of broadband noise (figure 9):

1. Loading fluctuations due to inflow turbulence interacting with the rotating blades.

2. The turbulent boundary layer flow over the airfoil surface interacting with the blade trailing edge.

3. Vortex shedding due to trailing edge bluntness.

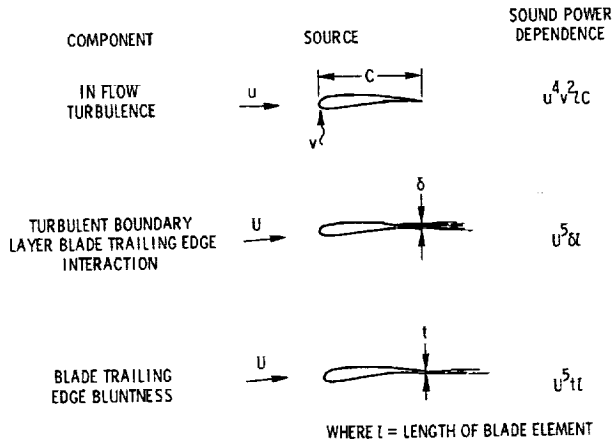

Figure 9. - Components of wind turbine broad band noise.

In contrast to the limited literature on wind turbine noise, the list of publications dealing with helicopter rotor noise is quite extensive. Although the concept of extracting energy from the flow by a wind turbine rotor is opposite of that of a helicopter rotor, which provides energy to the flow, the noise generating mechanisms show many similarities and an analogy between the two concepts is justified.

Inflow Turbulence

When the wind turbine rotor blades move through the turbulent air they encounter atmospheric inhomogeneities causing effective angle of attack changes which result in unsteady airfoil loading. This fluctuating force mechanism is a well known source for airfoil and helicopter rotor noise as decribed in References 19 and 20-42. To enable utilization of theoretical analyses from the literature for turbulent inflow source mechanisms applicable to helicopter rotors the contrast with wind turbine rotor mechanisms has to be discussed. When encountering inflow turbulence a helicopter rotor will ingest the turbulent eddy with a convection speed V_c, while for a wind turbine the eddy is blown into its rotor disc with a windspeed V_w. Downstream of the rotor plane of the wind turbine the flow is slowed down and the eddy is compressed. The lifting rotor of a helicopter accelerates the flow and the eddies are elongated. If the eddies are compressed rather than elongated and if the blade passage frequency is kept constant, the occurence of blade loading correlation due to the chopping of a single eddy by more than one blade is reduced.

Turbulence Characteristics The length scale and the intensity of the inflow turbulence are dependent on meteorological conditions and height above the ground (Ref. 43). A helicopter flying at different altitudes will thus encounter different turbulence conditions, while for any given wind turbine the distance above the ground is fixed. For the wind turbines considered here the turbulence might be considered isentropic which means that fluctuations are approximately the same in all directions (Ref. 44). For horizontal axis wind turbine generators the longitudinal turbulence component is by far most important. This longitudinal component is assumed to be a horizontal sinusoidal gust of the form:

$$w = \bar{w}\, e^{i\omega(t-x/V_w)} \qquad (1)$$

where $\bar{w}$ is the square root of the root mean square turbulence intensity, ω is the rotational frequency, t is the time and x corresponds to a chordwise distance. The wind structure is strongly dependent on temperature gradient and turbulence ordinarily is stronger in the daytime than at night when the atmosphere is more stable. In this paper a standard day is assumed with a negative temperature gradient as a function of height above the ground. The root mean square turbulence intensity at elevation h is given by (Ref. 45):

$$\bar{w}^2 = \int \Phi_x \, d\omega \qquad (2)$$

where Φ_x is the longitudinal turbulence spectrum at that elevation and is expressed in terms of a reference turbulence intensity w_r (Ref. 45):

$$\Phi_x(\eta, V_w) = \frac{w_r^2}{\omega}\left[\frac{.164\ \eta/\eta_o}{1+.164\ (\eta/\eta_o)^{5/3}}\right] \qquad (3)$$

where η is the reduced frequency $\frac{\omega h}{V_w}$ and η_o has the value of .0144 for a longitudinal gust. An expression for the reference turbulence intensity w_r as used in the structural analysis of the MOD-2 machine can be obtained from Reference 45:

$$w_r = .2\left[2.18\ V_w h^{-.353}\right]^{\frac{1}{1.185-.193\log h}} \qquad (4)$$

Substitution of Equation (3) in (2) yields, after integration, the root mean square turbulence intensity as a function of only windspeed and height above the ground:

$$\bar{w}^2 = w_r^2\left[hw_r/\{V_w\ R(w_r-.014\ w_r^2)\}\right]^{-2/3} \qquad (5)$$

where w_r is given by Equation (4). The longitudinal turbulence spectrum Φ_x has been integrated between a minimum frequency which was choosen very close to zero and a maximum frequency ω_{max} which was chosen such that high frequency (small extent) turbulence may be disregarded (Ref. 45).

Far-Field Noise Prediction - The induced fluctuating force $\frac{\partial F}{\partial t}$ per unit span is related to the horizontal gust by the aerodynamic transfer function G(k):

$$\left(\frac{\overline{\partial F}}{\partial t}\right)^2 = \omega^2 \overline{w}^2 \, e^{2i\omega(t-x/V_w)} \left|G(k)\right|^2 \qquad (6)$$

where $k = (\omega c_o/2V_w)$ and G(k) is based on Osborne's asymptotic solution for the compressible extension of the Sears function (Refs. 28 and 35), which for low frequencies is approximated by:

$$G(k) = \frac{\pi\rho U c dr}{1+2\pi k} \qquad (7)$$

Lighthill has shown that the sound pressure due to a fluctuating force F_i at a point with coordinates x_i (i=1,2,3) is given by the expression (Ref. 46):

$$p(t)-p_o = \frac{x_i}{4\pi r_o^2}\left[\frac{1}{c_o}\frac{\partial F_i(t-r_o/c_o)}{\partial t} + \frac{1}{r_o}F_i(t-r_o/c_o)\right] \qquad (8)$$

where c_o is the speed of sound and r_o is the distance between the source and receiver. If the source is considered to be a point dipole and the wavelength of the radiated sound is much smaller than the distance r_o to the receiver the expression for the acoustic pressure in the far field formulated by Curle (Ref. 47) may be used:

$$p(\bar{r},t) = \frac{\sin\phi}{4\pi c_o r_o}\int \frac{\partial F(t-r_o/c_o)}{\partial t} \qquad (9)$$

where $\bar{r}$ is the vector from the origin to the receiver location (in the y-z plane) and ϕ is the angle between r_o and the z-axis. Substituting Equations (6) and (7) into Equation (9) yields after integration and squaring the mean square sound pressure in the far field as being proportional to:

$$\left|p^2\right| = \frac{K_1(f)\, B \sin^2\theta\, \rho^2 c R\, \bar{w}^2\, U^4}{r_o^2\, c_o^2} \qquad (10)$$

where B is the number of blades, R is the radius of the rotor, and $K_1(f)$ is a frequency dependent scaling factor. To evaluate this scaling factor, the wind turbine rotor has been modeled as a dipole point source located at the hub and Equation (10) is compared with frequency spectra from the MOD-2 machine for which the noise was largely due to turbulent inflow (Refs. 15 and 16). The location of the peak intensity in the frequency domain is strongly dependent on blade velocity and longitudinal scale of turbulence (Ref. 24). The turbulence is dependent on height above the ground for non-varying meteorological conditions. To account for different hub heights as well as different rotor diameters the location of the peak intensity in the frequency domain is given by:

$$f_{peak} = S\, U/(h - .7R) \qquad (11)$$

where S is the applicable Strouhal number which is obtained from comparison with the measured MOD-2 noise spectra.

Power Output and Windspeed - If the power generated by the wind turbine is known rather than the wind speed, which is needed as input for Equations (4) and (5), it is necessary to know their relationship to enable noise predictions. Reference 48 suggests that for constant rotational speed machines the output power is linearly proportional to the windspeed velocity and pitch angle. Between the cut-in speed and the rated wind speed the power output will vary approximately linearly with windspeed, which can be expressed by the equation:

$$V_w = \frac{P}{P_r}(V_{ra}-V_{ci}) + V_{ci} \qquad (12)$$

where P_r is rated power output at the corresponding rated windspeed V_{ra} and V_{ci} is the cut-in windspeed at which no output power is produced. Equations (4), (5), (10), (11) and (12) are utilized to predict the noise spectra due to inflow turbulence for other machines and operating conditions.

Turbulent Boundary Layer-Trailing Edge Interaction

Noise is generated when the blade attached turbulent boundary layer convects into the wake at the trailing edge. Theoretical models of this trailing edge noise for helicopter blades are presented in References 20-22 and 48-60. The experimental and theoretical study in Reference 53 concludes that the trailing edge noise radiated from a local blade segment can be predicted by a first principles theory, which includes local Mach number, boundary layer thickness, length of the blade segment and observer position. A scaling law approach then was used for comparison with the noise radiation data from a stationary two-dimensional isolated airfoil segment. This theory will be utilized to predict the trailing edge noise generated by the blades of large horizontal axis wind turbine generators.

The scaling law prediction of Reference 53 gives for the trailing edge noise spectrum for an isolated airfoil:

$$SPL_{1/3} = 10 \log \left\{K_2 U^5 B\bar{D}\frac{\delta s}{r_o^2}\left(\frac{S}{S_{max}}\right)^4\left[\left(\frac{S}{S_{max}}\right)^{1.5}+0.5\right]^{-4}\right\} \qquad (13)$$

where $SPL_{1/3}$ is the one-third octave band sound pressure level, U is the local free stream velocity, B is the number of blades, δ is the local boundary layer thickness, s is

the airfoil span, r_o the distance to the receiver, $\bar{D}$ the directivity, S the Strouhal number and K_2 is a constant which equals 220 when SI units are used. Equation 13 is essentially the trailing edge noise prediction for a two-dimensional lifting surface in a uniform inflow. To predict the trailing edge noise from a rotating blade the blade is divided into small blade segments, with a length s, each experiencing a different local free stream velocity and each contributing to the noise at the receiver location. Because of the rotation this noise spectrum then is averaged around the azimuth. The local free-stream velocity U_x is given by:

$$U_x = 2\pi\ r_x\ n \tag{14}$$

where r_x is the distance from the local blade section to the center of the hub and n denotes revolutions per second. The thickness of the turbulent boundary layer at the trailing edge of the airfoil may be approximated by the turbulent boundary layer thickness of a flat plate which is given by (Ref. 62):

$$\delta = .37\ c_x\ /\ (R_{N_x})^{.2} \tag{15}$$

where c_x is the chord at radius r_x from the hub and R_{N_x} is the local Reynolds number. Assuming a linearly tapered rotor blade and neglecting twist, c_x can be expressed in terms of the root chord (c_r), tipchord (c_t), radius (r_x) and blade diameter (D):

$$c_x = c_t + \left(1- \frac{2r_x}{D}\right)\ (c_r-c_t) \tag{16}$$

The local Reynolds number is defined by:

$$R_{N_x} = \frac{U_x c_x}{\nu} \tag{17}$$

where ν is the kinematic viscosity. The directivity pattern of the radiated trailing edge noise, for an observer in the vertical (y=0) plane perpendicular to the rotor plane is given by dipole like behavior from Reference 53:

$$\bar{D}(\theta,\tfrac{\pi}{2}) = \frac{\sin^2\theta}{(1+M\cos\theta)^2\left[1+(M-M_c)\cos\theta\right]^2} \tag{18}$$

where θ is the angle between the source-observer line and its projection in the ground plane. The convection Mach number of the turbulence, M_c, is set to an average value of .8 M as suggested in Reference 53. To correct for the directivity of the source outside the y=0 plane, the source is assumed to be a dipole radiator in those directions and the directivity function is the one proposed by Fink (Ref. 63):

$$\bar{D}\ (\theta,\psi) = \sin^2\psi\ \bar{D}(\theta,\tfrac{\pi}{2}) \tag{19}$$

where ψ is the angle between the source-observer line and its projection in the y=0 plane. The Strouhal number in Equation 13 is defined as the ratio of frequency (f) times the boundary layer thickness (δ) and the undisturbed free stream velocity (U_x):

$$S = \frac{f\delta}{U_x} \tag{20}$$

The peak Strouhal number, S_{max}, associated with trailing edge noise equals .1 (Refs. 63-65 and 53). Although a different value is reported in Reference 52, in the present study a value S_{max}=.1 is adopted.

Trailing Edge Bluntness Vortex Shedding Noise

Vortex shedding behind the trailing edges of thick struts has been studied in References 54-56. This phenomenon produces noise as the coherent vortex shedding causes a fluctuating surface pressure differential across the trailing edge. This was established in Reference 52 as being an important source of self-noise for airfoils with blunt trailing edges. The vortex shedding frequencies observed in References 54-56 had a peak Strouhal number of about .24 when based on the trailing edge thickness and a velocity dependence of approximately U_x^6. This peak Strouhal number compares well with the ones found by other researchers who studied the vortex shedding behind wings, flat plates and circular and noncircular bodies (Refs. 23, 49, 52, and 57-60). In all cases, the turbulent boundary layer displacement thickness (δ^*) is much smaller than the characteristic dimension (t) from which the vortices are shed ($t/\delta^*>40$). Experimental results from noise measurements on several trailing edge configurations in the NASA Langley Quiet-Flow Facility, however, indicated that for a trailing edge bluntness of equal thickness or smaller than the displacement thickness of the boundary layer a Strouhal number of .1 is applicable (Ref. 52). It was shown that the overall sound pressure level of the noise generated at the blunt trailing edge follows a $U_x^{5.3}$ dependence. Using the directivity pattern presented in Reference 53, the following scaling laws are derived for the one-third octave band sound pressure levels in the acoustic far field:

for $t/\delta^* > 1$:

$$SPL_{1/3} = \frac{K_3 B U_x^{\ 6} t\ s\ \sin^2\theta\ \sin^2\psi}{1 + M\cos\theta} \tag{21}$$

and

$$f_{max} = .25\ \frac{U_x}{t+\frac{\delta_x}{4}} \tag{22}$$

for $t/\delta^* < 1$:

$$SPL_{1/3} = \frac{K_4 B U_x^{\ 5.3}\ t\ s\ \sin^2\theta/2\ \sin^2\psi}{(1+M\cos\theta)^3\left\{1+(M-M_c)\cos\theta\right\}^2} \tag{23}$$

and

$$f_{max} = .1 \frac{U_x}{t} \qquad (24)$$

where K_3 and K_4 are scaling constants. The constant K_4 has been obtained by comparing Equation (23) with the blunt trailing edge noise measurements from Figure 40 in Reference 52, which were first converted to one-third octave band data. The constant K_3 has been determined by equating Equation (21) and (23) for the case that the trailing edge bluntness is of the same thickness as the displacement thickness of the turbulent boundary layer. For most practical purposes the displacement thickness and the boundary layer thickness are related by:

$$\delta^* = \frac{\delta}{8} \qquad (25)$$

Equations (21) through (25) are used to predict the noise from wind turbine blades with blunt trailing edges using the same calculation procedure as for turbulent boundary layer trailing edge interaction noise.

To assess the relative importance of all three major aerodynamic noise sources (figure 9) predictions have been made for a MOD-2 machine at a distance of 100 m on-axis. The noise contributions due to turbulent inflow, trailing edge bluntness and turbulent boundary layer trailing edge interaction relative to the total noise is depicted in Figure 10. The turbulent inflow related noise dominates the spectrum at the low frequencies and is broad in character while turbulent boundary layer trailing edge interaction noise becomes relatively more and more important when moving up the frequency scale. Noise due to trailing edge bluntness is confined to a more restricted frequency band with its center frequency related to the thickness of the trailing edge. All predictions are limited to the acoustic far field, on-axis and without distinction between upwind and downwind directions as no propagation effects are incorporated.

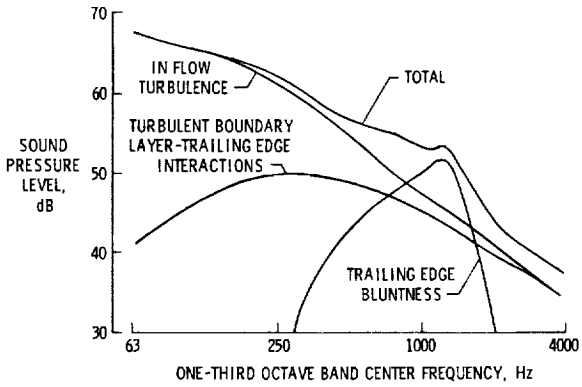

Figure 10. - On-axis broad band noise component predictions for the MOD-2 machine. (V_w = 9.8 m/s, P = 1500 kW, r = 100 m.)

COMPARISONS BETWEEN PREDICTIONS AND MEASUREMENTS

To show that reasonable agreement can be obtained between broadband noise predictions and far field noise measurements, comparisons have been made for four horizontal axis wind turbines with quite different physical characteristics (Figures 1 and 2). Also various distances, number of blades and power outputs are shown to give a good comparison with actual measured data. Figure 11 shows predictions and measurements for two downwind machines, MOD-0A and WTS-4, at different distances and different power outputs. Only the noise due to turbulent inflow is dependent on the actual power output (actually the turbulence intensity) as evidenced by the results depicted in Figure 11. Other noise source mechanisms are only dependent on rotational speed. The effect of the trailing edge bluntness of the three blades of the U.S. Windpower machine is shown in Figure 12 where the sharp peak around 2000 Hz in the noise spectrum disappears after the trailing edges have been sharpened.

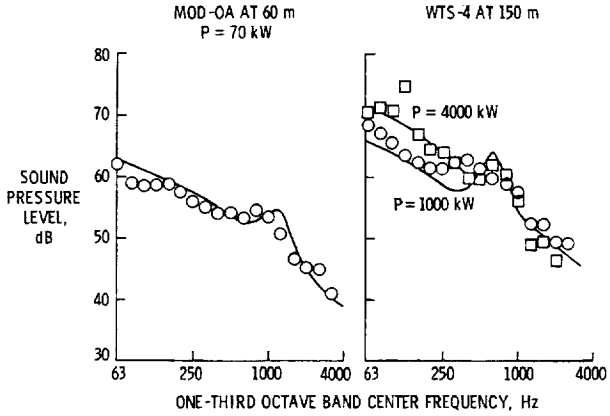

Figure 11. - Comparisons of measured and predicted on-axis broad band noise spectra for two downwind machines.

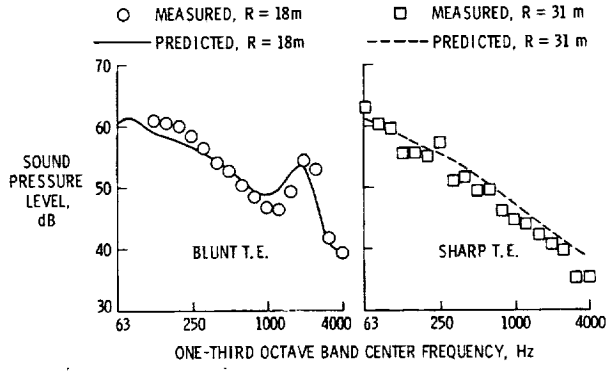

Figure 12. - Comparisons of measured and predicted broad band noise spectra for two different blade trailing edge configurations of the U.S. windpower inc. machine.

The predicted noise spectrum of a MOD-2 upwind machine at rated power is depicted in Figure 13 along with measured data points showing good agreement. In the same figure a broadband noise prediction is presented for a MOD-5B machine, at rated power, on axis, 200 m away from the hub. The difference is shown for a machine with sharp trailing edges and for the case that the blade trailing edges have the same bluntness as the MOD-2 machine. The noise signature of the MOD-5B is predicted to be 2-3 dB higher than the MOD-2 over the whole frequency range, both operating at rated power.

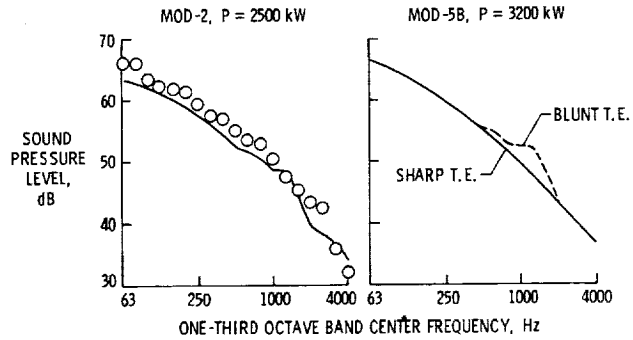

Figure 13. - Predicted on-axis broad band noise spectra for two upwind machines. (r = 200 m.)

CONCLUDING REMARKS

Noise measurements and observations have been presented for four large horizontal axis wind turbine generators with quite diferent characteristics in size and configuration. Effects of output power, directional radiation effects (up-, down-, and cross wind) and noise perception distances have been discussed based on field measurements. A method has been presented for predicting the broadband noise spectra of horizontal-axis, constant rotational speed machines, based on contributions from noise due to inflow turbulence, turbulent boundary layer-trailing edge interaction noise and noise due to a blunt trailing edge. Good agreement is shown between predictions and far field noise measurements of the four large wind turbine generators for various operating conditions. The prediction method includes the effects of distance from the machine, output power (windspeed), number of blades and tower and blade geometry. Broadband noise is predicted only on-axis and the method does not distinguish between upwind and downwind. Propagation effects other than distance are not included in the present prediction formulation.

REFERENCES

1. Hubbard, H.H., Shepherd, K.P., Grosveld, F.W.: Sound Measurements of the MOD-2 Wind Turbine Generator. NASA CR 165752, July 1981

2. Shepherd, K.P. and Hubbard, H.H.: Sound Measurements and Observations of the MOD-OA Wind Turbine Generator. NASA CR 165856, February 1982

3. Shepherd, K.P. and Hubbard, H.H.: Measurements and Observations of Noise from a 4.2 Megawatt (WTS-4) Wind Turbine Generator. NASA CR 166124, VA, May 1983

4. Hubbard, H.H. and Shepherd, K.P.: Noise Measurements for Single and Multiple Operation of 50 kW Wind Turbine Generators. NASA CR 166052, December 1982

5. Grosveld, F.W., Shepherd, K.P. and Hubbard, H.H.: Radiation of Aerodynamic Sound from Large Wind Turbine Generators. Proceedings of Inter-Noise '82, pp. 323-326, San Francisco, May 17-19, 1982

6. Hubbard, H.H., Grosveld, F.W., and Shepherd, K.P.: Noise Characteristics of Large Wind Turbine Generators. Noise Control Engineering Journal, Vol, 21, No. 1, pgs. 21-29, 1983

7. Stephens, D.G., Shepherd, K.P., Hubbard, H.H. and Grosveld, F.W.: Guide to the Evaluation of Human Exposure to Noise from Large Wind Turbines. NASA TM 83288, March 1982

8. Shepherd, K.P., Grosveld, F.W. and Stephens, D.G.: Evaluation of Human Exposure to the Noise from Large Wind Turbine Generators. Noise Control Engineering Journal, Vol. 21, No. 1, pgs. 21-29, 1983

9. Balombin, J.R.: An Exploratory Survey of Noise Levels Associated with a 100 kW Wind Turbine. NASA TM 81486, 1980

10. Greene, G.C. and Hubbard, H.H.: Some Calculated Effects of Non-Uniform Inflow on the Radiated Noise of a Large Wind Turbine. NASA TM 81813, 1980

11. Kelley, N.D.: Acoustic Noise Generation by DOE/NASA MOD-1 Wind Turbine. Proceedings of the Second DOE/NASA Wind Turbine Conference, Cleveland, Ohio, February 24-26, 1981

12. Martinez, R., Widnall, S.E. and Harris, W.L.: Predictions of Low-Frequency Sound from the MOD-1 Wind Turbine. FDL Report No. 80-5, MIT, 1980

13. Savino, J.M., Wagner, L.H. and Sinclair, D.M.: Wake Characteristics of an Eight-Leg Tower for a MOD-0 Type Wind Turbine. DOE/NASA 1038-77/14, Department of Energy, December, 1977

14. Thompson, D.W.: Analytical Studies and Field Measurements of Infrasound Propagation at Howard's Knob, N.C. Dept. of Meteorology, Penn State University, Final Report 18, September, 1980

15. Wells, R.J.: MOD-1 Wind Turbine Generator Noise Studies. Corporate Research and Development Report, General Electric Company, Schenectady, N.Y., October, 1980

16. Viterna, L.A.: The NASA LeRC Wind Turbine Sound Prediction Code. Proceedings of the Second DOE/NASA Wind Turbine Conference, Cleveland, Ohio, February 24-26, 1981

17. Keast, D.N. and Potter, R.C.: A Preliminary Analysis of the Audible Noise of Constant Speed, Horizontal-Axis Wind Turbine Generators. DOE/EV-0089, UC-11, 60, July 1980

18. Kelley, N.D.: Noise Generated by Large Wind Turbines. Presented at Wind Energy Technology Conference, Kansas City, MO, March 16-17, 1981

19. George, A.R. and Chou, S.T.: Comparison of Broadband Noise Mechanisms, Analyses, and Experiments on Helicopters, Propellers, and Wind Turbines. AIAA Paper No. 83 0690 presented at the 8th Aeroacoustics Conference, Atlanta, Georgia, April 11-13, 1983

20. George, A.R.: Helicopter Noise: State of the Art. AIAA Journal of Aircraft, 15, (11), pp. 707-715, Nov. 1978

21. Schlinker, R.H. and Brooks, T.F.: Progress in Rotor Broadband Noise Research. Preprint #A-82-38-51-D, Presented at the 38th Annual Forum of the American Helicopter Society, Anaheim, CA, May 4-7, 1982

22. Ffowcs Williams, J.E. and Hall, L.H.: Aerodynamic Sound Generation by Turbulent Flow in the Vicinity of a Scattering Half-Plane. Journal of Fluid Mechanics 40, pp. 657-670, 1970

23. Berger, E. and Wille, R.: Periodic Flow Phenomena. American Rev. Fluid Mech. 4, 313, 1972

24. Aravamudan, K.S., Lee, A. and Harris, W.L.: A Simplified Mach Number Scaling Law for Helicopter Rotor Noise. Journal of Sound and Vibration, Vol. 57, No. 4, pp. 555-570, 1978

25. Amiet, R.K.: Noise Due to Rotor-Turbulence Interaction. NASA CP 2052, May 1978

26. Aravamudan, K.S., Lee, A. and Harris, W.L.: Wind Tunnel Investigations of Model Rotor Noise at Low Tip speeds. International Specialists Symposium on Helicopter Acoustics, NASA Langley Research Center, Hampton, VA, May 22-24, 1978

27. Brown, D. and Ollerhead, J.B.: Propeller Noise at Low Tip Speeds. AFAPL-TR-71-35, September 1971

28. Osborne, C.: Unsteady Thin Airfoil Theory for Subsonic Flow, AIAA Journal, Vol. 11, pp. 205-209, Feb. 1973

29. Ffowcs Williams, J.E. and Hawkings, D.L.: Theory Relating to the Noise of Rotating Machinery, Journal of Sound and Vibration, Vol. 10, pp. 10-21, 1969

30. SenGupta, G.: Analysis of Jet-Airframe Interaction Noise, AIAA Paper 83-0783, 8th Aeroacoustics Conference, Atlanta, GA, April 1983

31. Amiet, R.K.: Acoustic Radiation from an Airfoil in a Turbulent Stream. Journal of Sound and Vibration, Vol. 41, No.4, August 1975

32. Whitfield, C.E.: An Investigation of Rotor Noise Generation by Aerodynamic Disturbance. NASA CR 157471, 1977

33. Leverton, J.W.: Helicopter Noise-Blade Slap. NASA CR 1221, October, 1968

34. Leverton, J.W.: The Noise Characteristics of a Large "Clean" Rotor. Journal of Sound and Vibration, Vol. 27, No. 3, April 1973

35. Homicz, G.F. and George, A.R.: Broadband and Discrete Frequency Radiation from Subsonic Rotors. Journal of Sound and Vibration, Vol. 36, No. 2, September 1974

36. Hayden, R.: Noise from Interaction of Flow with Rigid Surfaces: A Review of Current Status of Prediction Techniques. NASA CR 2126, October 1972

37. Sharland, I.J.: Sources of Noise in Axial Flow Fans. Journal of Sound and Vibration, Vol. 1, No. 3, pp. 302-322, 1964

38. Lowson, M.V. and Ollerhead, J.B.: A Theoretical Study of Helicopter Rotor Noise. Journal of Sound and Vibration, Vol. 9, pp. 197-222, March 1969

39. Lowson, M.V., Whatmore, A.R. and Whitfield, C.E.: Source Mechanisms for Rotor Noise Radiation. NASA CR 2077, August, 1973

40. Paterson, R.W. and Amiet, R.K.: Noise of a Model Helicopter Rotor Due to Ingestion of Turbulence. NASA CR 3213, November, 1979

41. Humbad, N.G. and Harris, W.L.: Model Rotor Low Frequency Broadband Noise at Moderate Tip Speeds. AIAA Paper 80-1013, June 1980

42. George, A.R. and Kim, Y.N.: High Frequency Broadband Rotor Noise. AIAA Journal, Vol. 15, No. 4, pp. 538-545, April 1977

43. Piercy, J.E., Embleton, T.F. and Sutherland, L.C.: Review of Noise Propagation in the Atmosphere. Journal of the Acoustic Society of America, Vol., 61, No. 6, June 1977

44. Ingard, U.: The Physics of Outdoor Sound. Proceedings of the 4th National Noise Abatement Symposium, 1953

45. Boeing Engineering and Construction: MOD-2 Wind Turbine System Concept and Preliminary Design Report. DOE/NASA 0002-80/2, July 1979

46. Lighthill, M.J.: On Sound Generated Aerodynamically; General Theory. Proceedings of the Royal Society, London, A 211, pp. 564-587, 1952

47. Curle, N.: The Influence of Solid Boundaries upon Aerodynamic Sound. Proceedings of the Royal Society, London, A 231, pp. 505-514, 1955

48. Anonymous: MOD-1 Windturbine Generator Analysis and Design Report. NASA CR 159495, General Electric Company, Space Division, March 1979

49. Chase, D.M.: Noise Radiated from an Edge in Turbulent Flow. AIAA Journal, Vol. 13, No. 8, August 1975

50. Amiet, R.K.: Effect of the Incident Surface Pressure Field on Noise Due to Turbulent Flow Past a Trailing Edge. Journal of Sound and Vibration, Vol. 57, pp. 305-306, 1978

51. Yu, J.D. and Tam, C.K.: An Experimental Investigation of the Trailing Edge Noise Mechanism. AIAA Journal, Vol, 16, No. 10, pp. 1045-1052, October 1978

52. Brooks, T.F. and Hodgson, T.H.: Prediction and Comparison of Trailing Edge Noise Using Measured Surface Pressures. AIAA Paper 80-0977, 6th Aeroacoustics Conference, Hartford, CT, June 4-6, 1980

53. Schlinker, R.H. and Amiet, R.K.: Helicopter Rotor Trailing Edge Noise. NASA CR 3470, Nov. 1981

54. Blake, W.K.: A Statistical Description of Pressure and Velocity Fields at the Trailing Edges of a Flat Strut. Report 4241, David W. Taylor Naval Ship Research and Development Center, Bethesda, MD, December, 1975

55. Blake, W.K., Maga, L.J. and Finkelstein, G.: Hydroelastic Variables Influencing Propeller and Hydrofoil Singing. Paper presented at the Winter Annual Meeting of ASME, Atlanta, GA, November, 1977

56. Blake, W.K. and Maga, L.J.: Near-Wake Structure and Unsteady Pressures at Trailing Edges of Airfoils. Reprint from Mechanics of Sound Generation in Flows, IUTAM/ ICA/AIAA Symposium, Gottingen, August 28-31, 1979

57. Krzywoblocki, M.Z.: Investigation of the Wing-Wake Frequency with Application of the Strouhal Number. Journal of the Aeronautical Sciences, Vol. 12, No. 1, January, 1945

58. Mendenhall, M.R., Spangler, S.B. and Perkins, Jr., S.C.: Vortex Shedding from Circular and Non-Circular Bodies at High Angles of Attack, AIAA Paper 79-0026, 17th Aerospace Sciences Meeting, New Orleans, January 15-17, 1979

59. Nishioka, M. and Sato, H.: Mechanism of Determination of the Shedding Frequency of Vortices Behind a Cylinder at Low Reynolds Numbers. J. Fluid Mech., Vol. 89, Part 1, pp. 49-60, 1978

60. Katz, J. and Weiks, D.: Behavior of Vortex Wakes from Oscillating Airfoils. AIAA Journal of Aircraft, Vol, 15, No. 12, December 1978

61. Howe, M.S.: A Review of the Theory of Trailing Edge Noise. Journal of Sound and Vibration, Vol. 61, No. 3, December, 1978

62. Schlichting, H.: Boundary Layer Theory. McGraw-Hill, Inc., Sixth Ed., 1968

63. Fink, M.R. and Schlinker, R.H.: Airframe Noise Component Interaction Studies. AIAA Journal of Aircraft, Vol. 17, No. 2, February 1980

64. Fink, M.R.: Noise Component Method for Airframe Noise, AIAA Journal of Aircraft, Vol. 16, No. 10, October 1979

65. Fink, M.R.: Airframe Noise Prediction Method. Federal Aviation Administration Report No. FAA-RD-77-29, March 1977 (available from DTIC as A039-664)